



HAL
open science

Effect of surface chemistry on the electrical double layer in a long-chain ionic liquid

Layla Bou Tannous, Mirella Simoes Santos, Zheng Gong, Paul-Henri
Haumesser, Anass Benayad, Agílio Pádua, Audrey Steinberger

► **To cite this version:**

Layla Bou Tannous, Mirella Simoes Santos, Zheng Gong, Paul-Henri Haumesser, Anass Benayad, et al.. Effect of surface chemistry on the electrical double layer in a long-chain ionic liquid. *Langmuir*, 2023, 39 (47), pp.16785-16796. 10.1021/acs.langmuir.3c02123 . hal-04161372v2

HAL Id: hal-04161372

<https://hal.science/hal-04161372v2>

Submitted on 30 Nov 2023

HAL is a multi-disciplinary open access archive for the deposit and dissemination of scientific research documents, whether they are published or not. The documents may come from teaching and research institutions in France or abroad, or from public or private research centers.

L'archive ouverte pluridisciplinaire **HAL**, est destinée au dépôt et à la diffusion de documents scientifiques de niveau recherche, publiés ou non, émanant des établissements d'enseignement et de recherche français ou étrangers, des laboratoires publics ou privés.

Copyright

The effect of surface chemistry on the electrical double layer in a long-chain ionic liquid

Layla Bou Tannous,^{†,‡} Mirella Simoes Santos,[†] Zheng Gong,[†] Paul-Henri Haumesser,[‡] Anass Benayad,[¶] Agilio A. H. Padua,[†] and Audrey Steinberger^{*,§}

[†]*Laboratoire de Chimie, École Normale Supérieure de Lyon, CNRS, 69364 Lyon, France*

[‡]*Univ. Grenoble Alpes, CEA, Leti, F-38000 Grenoble, France*

[¶]*Univ. Grenoble Alpes, CEA, Liten, F-38000 Grenoble, France*

[§]*Univ Lyon, ENS de Lyon, CNRS, Laboratoire de Physique, F-69342 Lyon, France*

E-mail: audrey.steinberger@ens-lyon.fr

Abstract

Room temperature ionic liquids (ILs) can create a strong accumulation of charges at solid interfaces by forming a very thin and dense electrical double layer (EDL). The structure of this EDL has important consequences in numerous applications involving ILs, for example in supercapacitors, sensors and lubricants, by impacting the interfacial capacitance, the charge carrier density of semi-conductors, as well as the frictional properties of the interfaces. We have studied the interfacial structure of a long chain imidazolium-based IL (1-octyl-3-methylimidazolium dicyanamide) on several substrates: mica, silica, silicon and molybdenum disulfide (MoS₂), using atomic force microscopy (AFM) experiments and molecular dynamics (MD) simulations. We have observed 3 types of interfacial structures for the same IL, depending on the chemistry of the substrate and the water content, showing that the EDL structure is not an intrinsic property of the IL. We evidenced that at a low water content, neutral and apolar (thus hydrophobic) substrates promote a thin layer structure, where the ions are oriented parallel to the substrate and cations and anions are mixed in each layer. In contrast, a strongly charged (thus hydrophilic) substrate yield an extended structuration into several bilayers, while a hetero-

geneous layering with loose bilayer regions was observed on an intermediate polar and weakly charged substrate and on an apolar one at a high bulk water content. In the latter case, water contamination favors the formation of bilayer patches by promoting the segregation of the long chain IL into polar and apolar domains.

Introduction

Ionic liquids (ILs) are an emerging class of ionic materials with melting points below 100 °C.^{1,2} Due to their remarkable properties such as low vapor pressure, wide electrochemical window, thermal stability, thermal conductivity, and other tunable properties,^{3,4} they have attracted a great deal of attention as liquid electrolytes for energy storage devices^{5,6} and ionic applications,⁷ and as lubricants or lubricant additives.^{8,9}

Compared to conventional electrolytes, ILs exhibit a denser interfacial structuring of the ions:^{10,11} cohesive interactions in ILs (Coulombian, van der Waals, hydrogen bonding, solvophobic)^{12,13} lead to a strong structural organization at solid and fluid interfaces.¹⁴⁻¹⁶ Ions can organize in mixed layers of cations or anions forming a checkerboard structure or in a lamellar structure with alternating layers of cations

and anions that can extend to several nanometers from the surface.¹⁷

Understanding the electrical double layer (EDL) structure adopted by the IL at the interface with a solid surface is of paramount importance for many applications because it impacts directly the performance of the devices. Indeed, in batteries and supercapacitors, the EDL structure controls the interfacial capacitance, and thus the maximal energy density.¹⁸ In iontronic devices such as IL-gated transistors, the IL is in contact with a semiconducting substrate. Modifying the EDL structure through an applied potential induces an extremely large conductivity change in 2D semiconducting layers or semiconducting nanowires, leading to the design of novel electronic devices and triggering advances in fundamental material sciences.^{19,20} Finally, the friction reduction across IL-based lubricants also directly depends on the interfacial structure.⁹ As a consequence, the friction coefficient can be tuned either by changing the number of ionic layers squeezed between smooth surfaces,^{21,22} or by changing the EDL structure through an applied potential.^{23,24} In order to rationalize the choice of the best IL/substrate combination for a given application, the scientific challenge is twofold: first, become able to predict the EDL structure depending on the liquid composition and the substrate's properties (chemistry, geometry, electrical potential...), and from that, as a second step, the resulting quantities of interest such as the interfacial capacitance, the conductivity of a semi-conductor, or the friction coefficient.

Experimentally, the EDL structure has been extensively studied by force spectroscopy techniques using either a surface force apparatus (SFA)^{10,25-28} or an atomic force microscope (AFM).²⁹⁻³¹ Nowadays, a direct assessment of the interfacial structure can be also provided through several advanced experimental techniques such as neutron reflectivity,^{28,32,33} surface-enhanced Raman spectroscopy,^{34,35} photo-emission electron spectroscopy,³⁶ or sum-frequency generation (SFG) spectroscopy.^{33,37,38} However, the AFM remains a method of choice for the direct investigation of IL interfaces. Thanks to its high sensitiv-

ity and versatility, it enables to investigate a wide variety of systems,³⁹ with recent developments toward an atomic-scale 3D mapping of the EDL.⁴⁰⁻⁴³

The EDL structure has also been widely investigated by molecular dynamics (MD) simulations, which provide key insights into the EDL structure and allow to scan the effect of the liquid composition and/or the substrate properties in well controlled numerical experiments.⁴⁴⁻⁴⁶ Some studies performed a further step, by also evaluating quantities of interest such as the interfacial capacitance⁴⁷ or the friction coefficient.^{48,49} However, MD results depend on the choices that are made to describe the interactions between the compounds, and thus need to be benchmarked against experimental findings. A few studies demonstrate an excellent correlation between simulated density profiles and AFM experimental results,^{31,35,42,50,51} providing a deep and reliable understanding of the investigated EDLs.

Previous studies have evidenced that for a given IL, the EDL structure depends on the substrate's chemical nature,^{52,53} its topology,^{49,54} and its surface charge.^{19,30,31,35,42} The presence of water contamination also matters, but depending on the system and the water concentration, it can either reinforce⁵⁵ or weaken^{56,57} the interfacial ordering, and the precise role of water remains often unclear.⁵⁸ The IL chemical composition is also crucial. For example, hydrogen bonding between ions produces a stronger interfacial nanostructure⁵⁹ and impacts their lateral organization.⁴³ The length of an alkyl side chain is an other important parameter, since a long apolar chain confers amphiphilic properties to the associated ion.¹⁷ As a result, long chain ILs have been shown to segregate into polar and apolar nanostructures in the bulk, that turn into a lamellar ordering in a succession of bilayers close to a solid surface in many systems.^{25,26,32,33,60} However, a recent MD simulation predicts a completely different organization into thin layers of ions oriented parallel to the substrate for a long chain imidazolium-based ionic liquid, 1-octyl-3-methylimidazolium dicyanamide (C₈mimDCA), on molybdenum

disulfide (MoS_2).⁴⁶ If confirmed experimentally, this behaviour is very interesting for two reasons. First, on the fundamental point of view, can we understand what controls the orientation of a long chain imidazolium based IL over different substrates? Second, there is so far a lack of studies of the EDL structure formed by ILs over MoS_2 , even though it is a 2D semiconductor of great interest for iontronic applications.⁶¹

In this work, we have combined AFM experiments and MD simulations in order to investigate the role of the surface chemistry on the interfacial organization of C_8mimDCA , and elucidate the influence of water contamination. We have chosen four different substrates with a low surface roughness: two standard hydrophilic substrates, mica and silica (SiO_2), and two hydrophobic substrates, silicon (Si) and MoS_2 . Complementary benchmark simulations were also performed with a short-chain imidazolium based IL. We first present AFM results that evidence major structural differences on different substrates. We then compare MD simulations on MoS_2 and SiO_2 with a pure and a wet IL, in order to clearly differentiate the effect of the surface chemistry from the one of water impurities. Finally, we compare the experimental and numerical results before rationalizing our findings.

Materials and Methods

Experiments

C_8mimDCA and 1-ethyl-3-methylimidazolium dicyanamide (C_2mimDCA) were purchased from Solvionic, France. They were dried using schlenk lines achieving a vacuum of 10^{-1} mbar. Water was evacuated by rotary evaporation (100 rpm) and heating (40°C) for approximately 4 days under argon atmosphere. After this, the water content was measured, using Karl Fischer titration, to be around 80 ppm for C_8mimDCA and 120 ppm for C_2mimDCA . The density ρ , viscosity μ , and ion pair diameter D of both ILs are given in Table 1. ρ was measured after the degassing using an U -tube oscillator

at different temperatures. μ was measured using a falling-ball viscometer. D was calculated from ρ assuming a cubic packing geometry according to the method described by Horn *et al.*¹⁰ The molecular weight (MW), dimensions, and molecular structure of the ions are summarized in Table 2. The sizes were calculated in flat, stretched configurations of the side chains as drawn in the last column of Table 2, using the GAFF force field with van der Waals radii from reference.⁶²

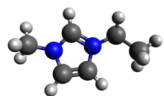
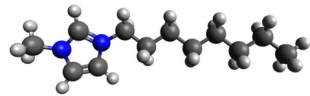
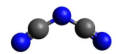
Table 1: Density ρ and viscosity μ at 25°C , and ion-pair diameter D of ILs considered in this work.

IL	ρ (g cm^{-3})	μ (mPas)	D (nm)
C_2mimDCA	1.10	13.3	0.65
C_8mimDCA	1.00	69.1	0.76

Atomically smooth muscovite mica was cleaved by using adhesive tape before each use. SiO_2 substrates are the native oxide layer of silicon wafers, while the Si substrates were obtained by removing this oxyde layer using a hydrofluoric (HF) treatment. X-ray Photoelectron Spectroscopy (XPS) data for both types of Si wafers are provided in the Supporting Information (Figure S1) to characterize the oxygen content at their surface. The MoS_2 substrate was prepared in the Cadot group at CEA-LETI. MoS_2 thin layers (2 nm-thick) were deposited on SiO_2/Si wafers (500 nm-thick thermally grown SiO_2) by atomic layer deposition in a 300 mm Trillium chamber (from Applied Materials) using the procedure reported in Cadot *et al.*⁶³ Subsequently, a post-deposition annealing under nitrogen was applied in order to crystallize the MoS_2 layer (5 min, 900°C , 1 atm in a Jipelec jetfirst RTP tool). The roughness of these substrates was checked to be low: maximum height of the profile $R_t < 1.3$ nm for a scan size of $1\ \mu\text{m}$. Typical AFM topography pictures of the four substrates are provided in Figure S2.

Force curves were collected using a JPK NanoWizard 4 AFM in contact mode, within a JPK fluid cell that was clamped over the substrate (see Figure 1). The sealing was ensured by compressing a Viton O-ring between the cell

Table 2: Molecular weight MW , dimensions, and molecular structure of the ions used in this study. Carbon atoms are shaded gray, nitrogen are blue, hydrogen are white.

Ion	MW (g mol ⁻¹)	Dimensions (L x W x H, Å)	Molecular structure
C ₂ mim	111.17	9.4 x 6.5 x 4.0	
C ₈ mim	195.32	16.7 x 6.5 x 4.0	
DCA	67.05	7.3 x 4.3 x 3.4	

and the substrate. Both the fluid cell and the O-ring were cleaned by sonication for 15 min in distilled water, followed by another 15 min sonication in ethanol, and then dried under argon prior to mounting. A silicon skirt fixed around the cantilever holder was laid upon the top of the fluid cell to reduce the exposure of the cell content to ambient air. The fluid cell comprised a gas inlet, a liquid inlet and a liquid outlet. It was flushed with dry nitrogen using the gas inlet prior to injecting the ionic liquid through the liquid inlet. Unless mentioned otherwise, the experiments were performed under a weak nitrogen flux in order to reduce the water uptake of the liquid. After the experiments, the IL was extracted through the liquid outlet and its water content was checked. The temperature within the fluid cell was approximately 25 °C.

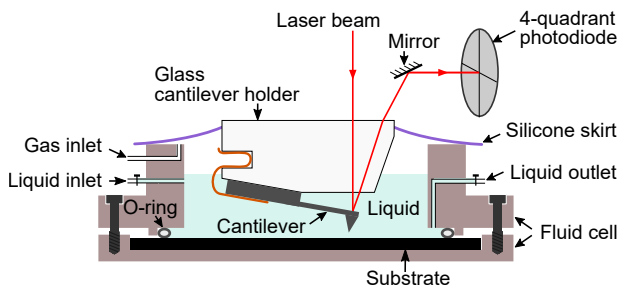


Figure 1: Sketch of the AFM setup within the fluid cell. The cantilever deflection was measured through the displacement of the laser spot on a 4-quadrant photodiode. The glass cantilever holder was mounted on a piezoelectric element, not represented on this sketch, that piloted its vertical motion.

For our measurements, we used contact mode cantilevers A from 4XC-NN OPUS AFM probes without coating. To avoid contamination, they were plasma cleaned for 30s prior to use and a new tip was used for each set of experiments. The manufacturer specifies a tip height of 14 μm, a tip radius ≤ 7 nm, and a spring constant of ≈ 0.3 N m⁻¹. The spring constants were calibrated in air far from the substrate using a contact-free method, with a relative uncertainty of 5%. In this method, the Sader calibration method was coupled with a thermal noise measurement around the first resonance of the cantilever to yield both the cantilever spring constant and the deflection sensitivity in air.⁶⁴ The AFM cantilever was then fully immersed in the IL. Its spring constant remained the same, but the sensitivity changed. The sensitivity in the IL was measured using the standard contact-based method, where the signal of the deflection sensor was recorded as a function of the vertical piezo displacement, and a straight line was fitted through the steepest region of the repulsive contact part of the curves. The maximal setpoint was about 40 nN.

The cantilever deflection versus piezo displacement curves were recorded with an approach velocity below 400 nm s⁻¹ to prevent dynamic effects due to viscous drag. We have checked that no viscous drag modified the curves below a velocity of 500 nm s⁻¹. The approach velocity and acquisition rate for each experiment are given in Table S1, together with the cantilever spring constant and the deflection sensitivity in the IL.

Typical start distances for the scan were 50–70 nm from the repulsive region. The applied force did not exceed 40 nN, however no layers were detected at forces greater than 10 nN, so that the maximal force setpoint was set at 10 nN in the reported approaches. Data were subsequently converted to force versus tip-substrate separation using Matlab scripts in which the baseline of zero force was set at the mean force far from the contact. The zero separation between the tip and the sample was defined as the median separation in the force range between 8 and 10 nN. For a statistical analysis, we recorded series of at least 10 force curves at the same position on the substrate with the same scan parameters.

Molecular dynamics simulations

Molecular dynamics (MD) simulations were performed to support the understanding of the interactions of C₈mimDCA with SiO₂ and MoS₂ surfaces, for the pure IL on the one hand and in the presence of water impurities on the other hand. C₂mimDCA, an ionic liquid with a short chain side-group on the imidazolium ring, was also simulated as a benchmark. A periodic slab geometry was used.

The ionic liquids C₂mimDCA and C₈mimDCA were described by the CL&Pol polarizable force field for ionic liquids⁶⁵ and water simulated using the SWM4-NDP polarizable model.⁶⁶ These force fields are based on the Drude induced dipole method. A small modification was made to ensure a better stability of the trajectories, namely: the Thole damping parameter was set to 1.8 instead of the usual 2.6, otherwise the DCA anions might undergo unrealistic conformational changes.⁴⁶ SiO₂ was modeled as crystalline silica and described by the ClayFF⁶⁷ force field, which uses fixed atomic partial charges and includes the presence of hydroxyl groups at the silica surface (see Supporting Information for details). MoS₂ was represented by a force field with a compatible functional form⁶⁸ with electrostatic interactions described by a fixed-potential surface, as in the recent work of Gong and Padua.⁴⁶ The van der Waals and electrostatic interactions

were truncated at 1.2 nm in direct space and the particle mesh Ewald approach was used to account for electrostatics at long-range, with a relative accuracy under 10⁻⁵. For the simulation of silica substrates with fixed-charge method, a slab correction was applied to remove artificial interactions between images in the z direction.⁶⁹

The simulation boxes were built by placing two xy -periodic slabs of MoS₂ with a spacing along z , and this space filled with the IL (and water, if present) in random positions and orientations within the slit pore. The numbers of ions and molecules inserted were determined in such a manner that the equilibrated distance between the two surfaces was close to 8 nm. Equilibrations were performed at constant NVT , and were assessed by monitoring the time evolution of the distance between two substrates and the distributions of ions, for each system. The distances reach equilibrium in less than 1 ns, while the distributions of ions could take more than 100 ns to stabilize. Once the systems equilibrated, production runs were carried out under the NVT ensemble, with the two slabs of MoS₂ allowed to move during the simulation. The same procedure was followed for the silica systems. In the humid systems, a concentration of 20 000 ppm of water was considered, which corresponds in the C₂mimDCA system to a molar ratio of 511:100 between IL and water, and in the C₈mimDCA system to a molar ratio of 312:100 between IL and water.

Simulations were ran using the OpenMM^{70,71} code, with production trajectories of at least 100 ns with a 1 fs integration timestep.

Results and Discussion

AFM measurements

We recorded force curves of C₈mimDCA on four different substrates: mica, SiO₂, Si, and MoS₂. Figure 2 displays 2D force-separation histograms generated from 10 force versus separation approach curves on each substrate. In this statistical representation, the number of data points recorded into each rectangular bin

in the force-separation plane is evaluated and color-coded. The bin size is 0.05 nN in force and 0.02 nm in separation. This representation, inspired by the work of Black *et al.*,³¹ allows to evaluate the repeatability of the curves and identify statistically robust features when individual curves differ.

On mica, very reproducible force-separation curves were recorded in the repeated approaches. No measurable force was acting on the tip at separations higher than ~ 6 nm, defining the zero force baseline. At smaller separations, two events composed by a force increase followed by a mechanical instability were observed. The force increase is interpreted as resulting from the compression of the interfacial nanostructure, while the mechanical instability reflects the ejection of a layer. These layers were $2.3 \text{ nm} \pm 0.1 \text{ nm}$ thick, thus thicker than the length of the cation and than the size of an ion pair (see Table 1), and thinner than what would be expected from a bilayer with a toe-to-toe configuration of straight and perpendicular octyl chains. This suggested that the ejected layers were bilayers with a chain interdigitation as proposed in Griffin *et al.*,³² and/or an orientational disorder of the long alkyl chains as suggested by MD simulations.⁷² The force required to rupture each layer increased as the tip moved closer to the surface. This can be explained by a decreased layering order further from mica as the molecular structure approached that of the bulk C₈mimDCA.

On HF treated Si and on MoS₂, no thick layers were observed. Below typically 2 nm, individual approach curves differed from each other (see example given in Figure S4). However, several thin layers appeared as statistically robust features (yellow to red areas) on the 2D histograms built from 10 successive approach curves (see the bottom row of Figure 2 and the zooms in Figure S5). Following the line of maximal number of points (ridge line), the robust features appeared in regions where the interfacial structure was compressed. They were separated by layer expulsion events that appeared as an abrupt change of slope of the ridge line and/or a blue to green segment with a locally lower number of counts. Most expulsion events

were also associated with a larger spread of the data points, reflecting a significant variability of the force level at expulsion. 1D separation histograms, which correspond to the projection of the 2D histograms on the separation axis, were a complementary tool to locate the layer expulsions,⁷³ as explained in the Supporting Information.

On MoS₂, 3 thin ionic layers, with a thickness of 0.3–0.4 nm, could be detected. The width of these layers was in good agreement with the dimension of the ions given in Table 2, if the imidazolium cations were oriented parallel to the substrate, and with the structure predicted by the simulations of Gong *et al.* on MoS₂.⁴⁶ However, in the AFM 2D histogram on MoS₂, the inner layer seemed to subdivide in two: layer 1b that started at a separation of about 0.5 nm from the substrate and was ejected at a force around 4 nN and a separation of about 0.3 nm, and layer 1a located at 0.2 nm, a very rigid (vertical) layer that yielded a little above 5 nN. The uncertainty of the distance was about 0.07 nm, so that layer 1b was compatible with both the ion’s height and the MD density profiles, while layer 1a was thinner.

3 thin layers were also detected on HF treated Si. They had a width of about 0.5 nm for the two outer layers and 0.8 nm for the inner one. These layers were wider than the layers on the MoS₂ substrate, but also implied a parallel orientation of the alkyl tails.

On silica, a third type of structure was observed, with one thick layer that was ejected at a separation of about 2 nm at a very low force level (a zoom is provided in Figure S5), and two thin layers below 1.2 nm, as indicated by the arrows on Figure 2 (top right panel). These layers had a thickness of about 0.5 nm, as the two outer layers on HF treated Si.

By studying the same IL on different surfaces, we demonstrated that the interfacial structure of a long chain IL is not an intrinsic quality of the IL, but also depends on other conditions including surface chemistry and/or IL water content. It is worth noting that at the end of the day, the water content of the IL was found to be around 10 000 ppm for the measurements on mica and SiO₂, showing that different struc-

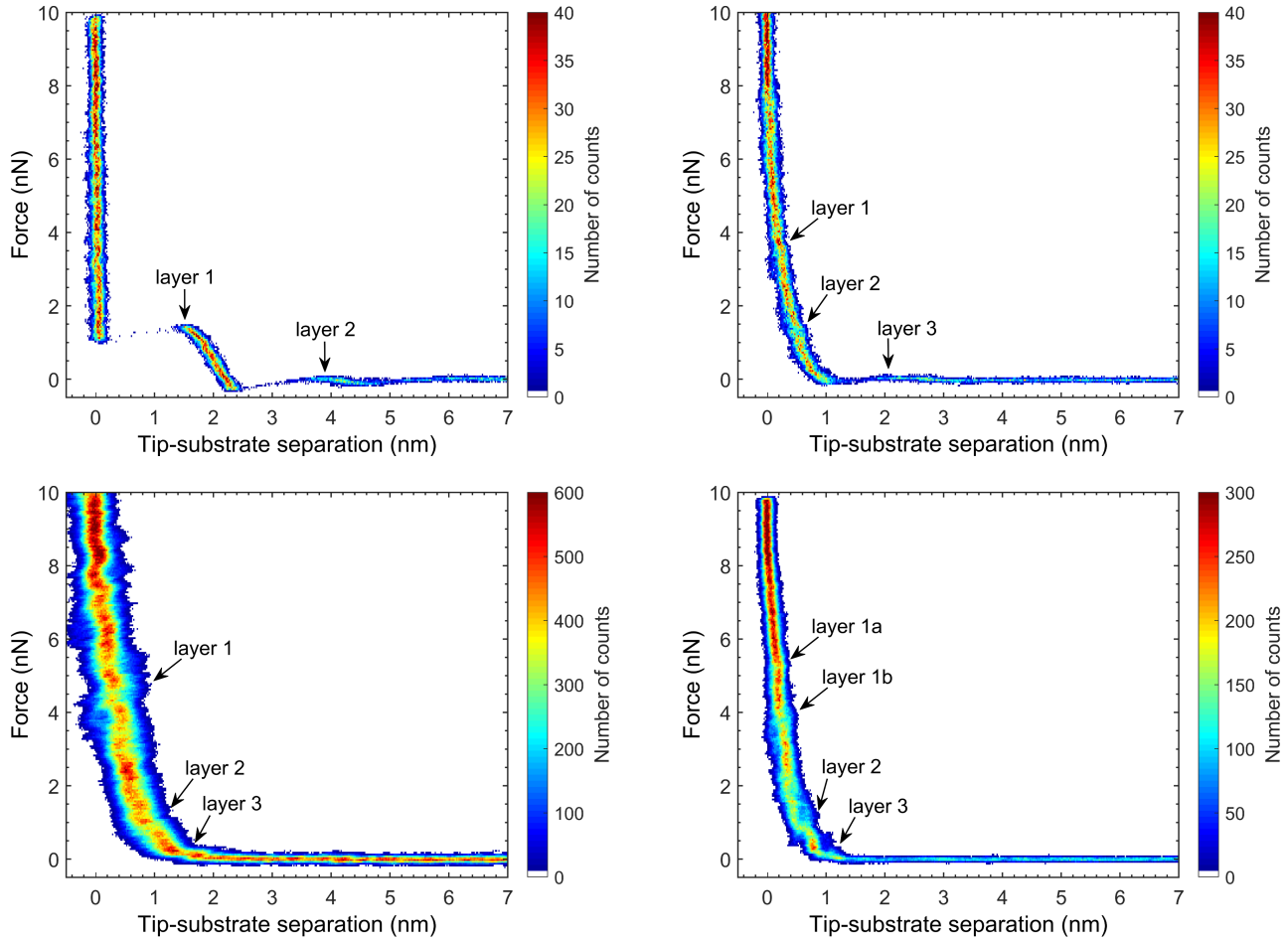


Figure 2: 2D force versus separation histograms for an AFM tip approaching different surfaces in C₈mimDCA, generated from 10 individual approach curves. Top left: mica. Top right: SiO₂. Bottom left: HF treated Si. Bottom right: MoS₂. The arrows point toward the ejection event of the designated layer.

tures were observed on different substrates at a similar bulk water content. However, the water content was lower in the other experiments: 2200 ppm on Si and 4000 ppm on MoS₂. The experimental bulk water contents are summarized in Table S1, both in ppm and as molar ratio.

In order to further check the influence of water impurities on the interfacial structures, we performed an additional experiment: we recorded force curves on MoS₂ in water rich C₈mimDCA. The system was left overnight under ambient conditions and force curves were recorded the next day, as the water content of the IL reached 40 000 ppm. Figure 3 shows a 2D histogram of 10 approach curves in this wet system. 3 thin layers were observed below 2 nm, as on the drier system, but their positions were shifted by 0.2 nm toward the left, as if layer 1a (defined on Figure 2, bottom left) was not ejected below the 10 nN setpoint, so that the separation zero was set on layer 1a instead of on the substrate. This shift was further evidenced by the comparison of the 1D separation histograms of the two systems, shown in Figure S6. This difference with water content, as well as the size of layer 1a, may be attributed to water molecules squeezed between the tip and the substrate. Remarkably, a faint thick layer also appeared at higher separation, very similar to the one observed on the silica substrate.

Molecular dynamics simulations

Molecular dynamics simulations were performed on MoS₂ and on silica, with and without water molecules, in order to clearly differentiate the influence of the surface chemistry from the influence of water impurities on the interfacial structure of the ILs.

Simulations on MoS₂. MD trajectories of 600 ns were obtained for C₂mimDCA and C₈mimDCA in an 8 nm wide slab system with MoS₂, pure and in the presence of 20 000 ppm of water, under a 0 V surface potential difference. Density profiles of the ions and water in the region between the surfaces are plotted in Figure 4 for the C₈mimDCA system. The corresponding curves for the C₂mimDCA sys-

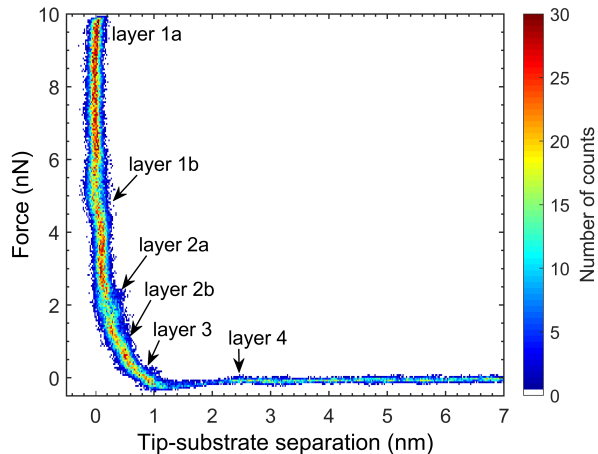


Figure 3: 2D force versus separation histogram generated from 10 individual approach curves in wet C₈mimDCA on MoS₂. The water content was 40 000 ppm. The arrows point toward the ejection event of the designated layer.

tem are reported in Figure S7. Figure 5 depicts simulation snapshots of the wet system for both ILs. Finally, angular distributions for the C₈mimDCA systems are represented in Figure 6.

In both dry systems, the density profiles in the pure ionic liquid were quite symmetric on the two surfaces (top curves), indicating a good equilibration of the simulated systems. They displayed three noticeable ordered layers at a distance below 1.8 nm from the substrate, with a similar thickness of 0.34–0.40 nm for both ILs. Note that this structure was in very good agreement with our experimental findings for C₈mimDCA (Figure 2, bottom right). The density profiles of anions and cations had coinciding maxima, meaning that cations and anions were mixed in each interfacial layer. In the C₈mimDCA system, a weak structuration into an apolar domain containing the alkyl chains, and a polar domain containing the DCA anions and the imidazolium heads, was additionally observed around 2 nm from the MoS₂ walls. This kind of feature was neither observed nor expected in the short-chain C₂mimDCA system.

In the presence of water molecules (bottom panel of Figure 4, and Figure 5), the behaviour of the short-chain and long-chain systems dif-

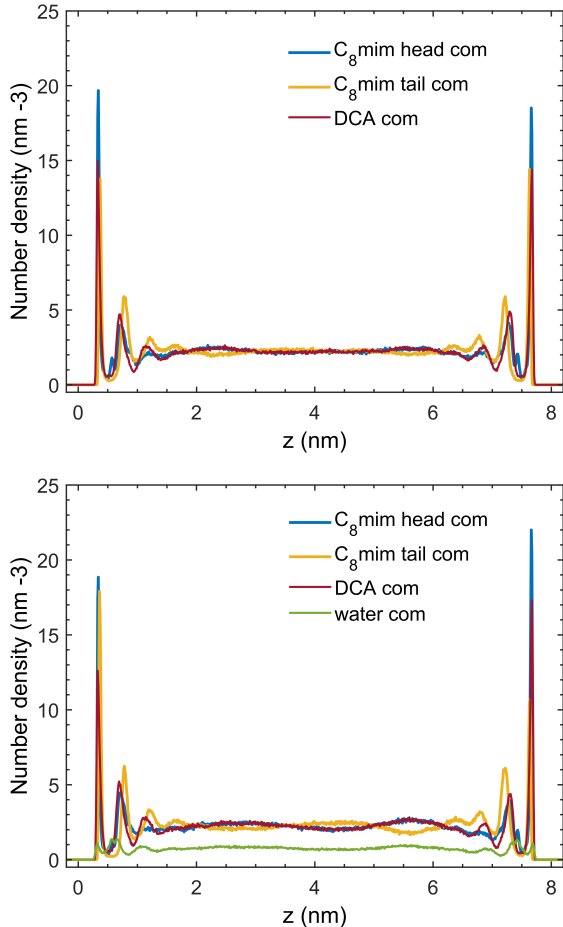


Figure 4: Density profiles of the $C_8\text{mimDCA}$ systems with MoS_2 . Plotted are the centers of mass (com) of the imidazolium head groups and of the alkyl tails of the $C_8\text{mim}$ cations, of the DCA anions, and of water molecules. The top plot corresponds to the dry system, whereas the bottom one contains 20 000 ppm of water. The top plot was adapted from Gong *et al.*,⁴⁶ with the permission of AIP Publishing.

ferred. While in the $C_2\text{mimDCA}$ system the addition of the water did not significantly modify the density profiles of the ionic species (see Figure S7), a marked asymmetry appeared in the $C_8\text{mimDCA}$ system. Does this asymmetry mean that the simulation was not fully converged in this system? This would be surprising, because one would expect the addition of water to decrease the viscosity of the IL, thus accelerating the dynamics rather than slowing it down. More probably the result of the simulation was representing either a stable or a deep metastable state of the system. In the

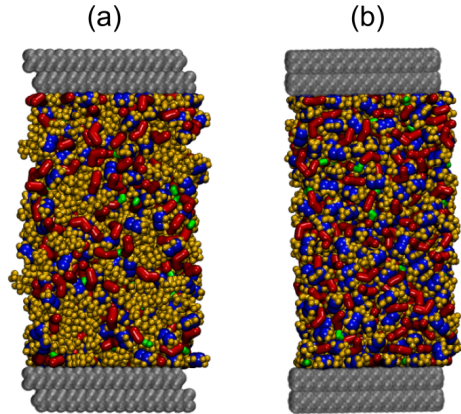


Figure 5: Snapshots of the simulation of (a) $C_8\text{mimDCA}$ and (b) $C_2\text{mimDCA}$ in a MoS_2 slit in the presence of water. The MoS_2 walls are represented in gray, water in green, DCA in red, the imidazolium heads in blue, and the alkyl chains in orange.

humid system, the segregation into polar and apolar domains at the right side of the slit became much stronger than in the dry system and propagated toward the left side of the slit, shifting slightly the center of the leftmost polar domain from 2.3 nm in the dry system to 2.7 nm. The position of the three thin ionic layers close to the walls remained the same as in the dry system, but a concentration difference appeared in the layers closest to the walls: the alkyl tails were depleted at the right wall and replaced by charged groups, whereas the reverse was observed in the peak closest to the left wall. Finally, the water density formed three small peaks at the inner edge of the three ionic peaks, oppositely from the alkyl chain peaks, and followed closely the density profile of the charged groups (imidazolium head-groups and anions) in the central part of the simulation cell, meaning that the water was found predominantly in association with the charged groups.

The concentration shifts in the inner ionic layers can be better understood by looking at the angular distributions of the head-group and alkyl chain of the cations, of the anions and of water molecules in the first ionic layer, plotted in Figure 6. The presence of water didn't affect the orientation of the charged groups, which were mostly parallel to the MoS_2 surface. How-

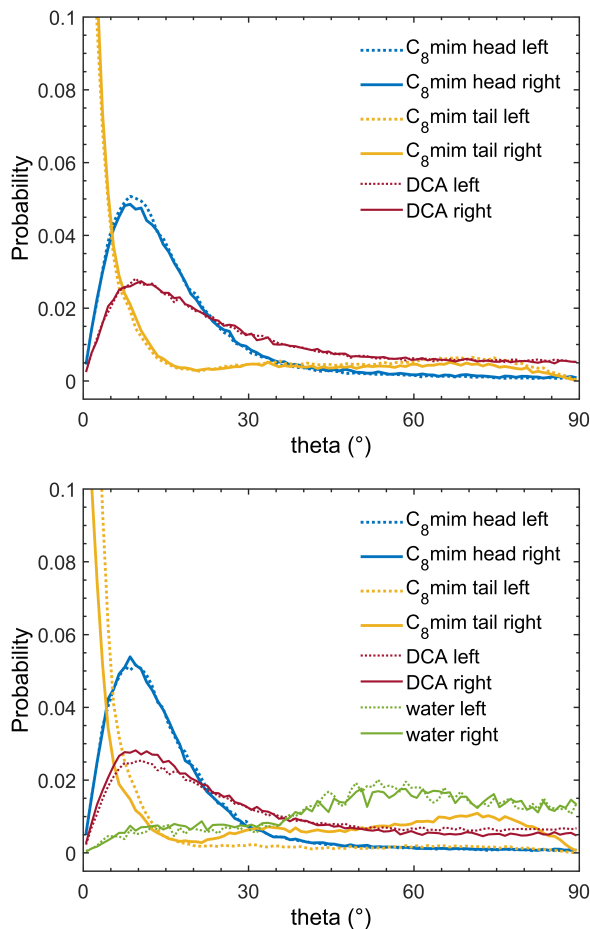


Figure 6: Angular distributions of the $C_8\text{mimDCA}$ systems with MoS_2 , for the ions located in the first layer close to the left and right wall. The angles plotted are between the plane of the imidazolium ring and the MoS_2 surface, between the end-to-end vector of the octyl side chain and the surface, and between the planes of the DCA anions and water molecules and the surface. The top plot corresponds to the dry system, whereas the bottom one contains 20 000 ppm of water. The top plot was adapted from Gong *et al.*,⁴⁶ with the permission of AIP Publishing.

ever, it modified the angular distribution of the alkyl tails. In the dry system, most of the alkyl tails of the cations lay parallel to the MoS_2 surface, as reported before,⁴⁶ with a few chains taking a 70° angle with respect to the substrate. In the presence of water, the asymmetry remarked before in the density profiles was also seen in the angular distributions of the alkyl tails. At the right wall, more tails assumed a 70° angle, liberating space close to the substrate for the charged groups, while at the left wall, all alkyl tails lay parallel to the wall.

Simulations on SiO_2 . MD simulations were also performed for $C_8\text{mimDCA}$ and $C_2\text{mimDCA}$ between silica surfaces with and without the presence of water. In both systems, the presence of water had no influence on the density profiles of the ions, as shown in Figure 7 for $C_8\text{mimDCA}$ and in Figure S7 for $C_2\text{mimDCA}$. When present, the water molecules aggregated in the vicinity of charged groups.

Interestingly, $C_8\text{mimDCA}$ and $C_2\text{mimDCA}$ assembled very differently from each other in these simulations, as shown in the snapshots presented in Figure 8. Both ILs also assembled differently in the silica slit and in the MoS_2 slit. In the $C_2\text{mimDCA}/\text{silica}$ system, the ions assembled into several thin layers on a similar range as on MoS_2 , but with a mismatch in the position of the density peaks of the anions and the charged head groups of the cations (Supporting Information). In the $C_8\text{mimDCA}/\text{silica}$ system, a strong segregation into apolar and polar domains was observed in the density profiles of Figure 7, independently of the presence of water. On the snapshot in Figure 8(a), a bilayer structure was observed on wide portions of the silica surfaces, but didn't span the entire width of the substrate. The density profiles of the charged groups were symmetric and displayed for both groups a first peak at 0.4 nm from the silica substrate. This peak was noticeably shorter and wider than its counterpart on MoS_2 . An even wider peak was located around 2.3 nm from the substrate, at the same distance than the much weaker polar domain observed for pure $C_8\text{mimDCA}$ on MoS_2 . This peak corresponded to the outer part of a bilayer structure,

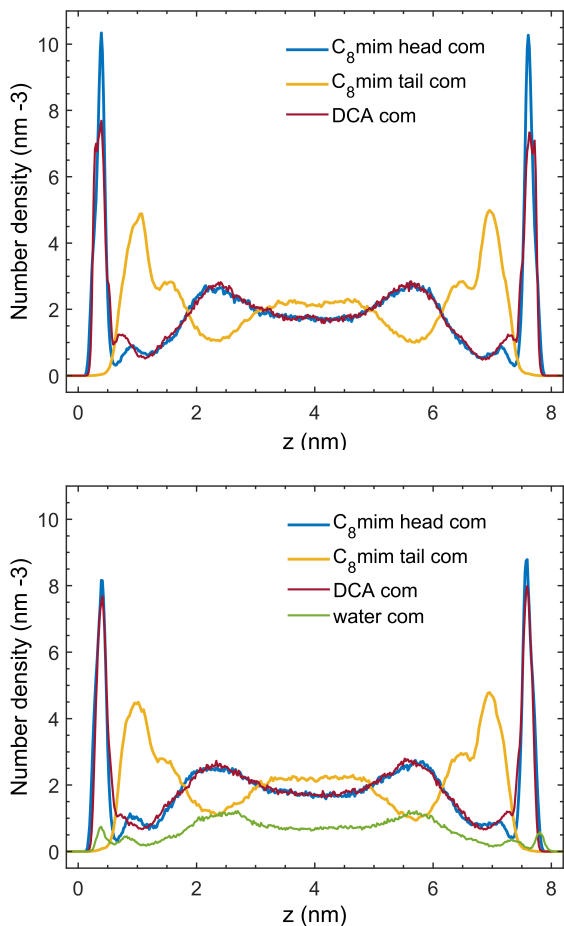


Figure 7: Density profiles of the $C_8\text{mimDCA}$ systems with SiO_2 . Plotted are the centers of mass of the imidazolium head groups of the $C_8\text{mim}$ cations, of the DCA anions, and of water molecules. The top plot corresponds to the dry system, whereas the bottom one contains 20 000 ppm of water.

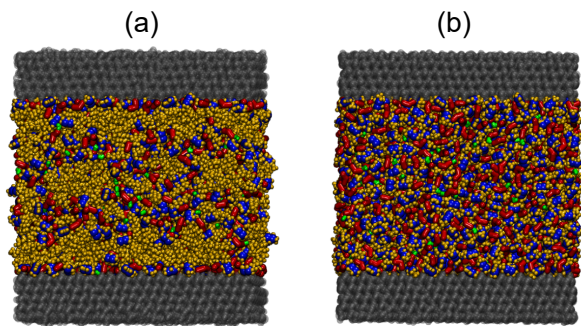


Figure 8: Snapshots of the simulation of (a) $C_8\text{mimDCA}$ and (b) $C_2\text{mimDCA}$ in a silica slit in the presence of water. The silica walls are represented in gray, water in green, DCA in red, the imidazolium heads in blue, and the alkyl chains in orange.

whose location matched well with the experimental bilayer width. A much smaller intermediate peak was present at 0.7 nm for the DCA anions and 0.9 nm for the imidazolium ring, reflecting the ionic structure in the small portions that were not covered by the bilayer close to the substrate.

The analysis of the angular distributions in the $C_8\text{mimDCA}/\text{silica}$ system showed that, in contrast with the MoS_2 system, the imidazolium ring and tail, as well as the DCA plane, adopted a broad range of orientations in the vicinity of the wall, as shown in Figure 9. The most probable configuration of the imidazolium ring and tail is however perpendicular to the silica surface. This angular distribution explained both the width and the location of the first density peak for the charged species in this system. The perpendicular configuration of the alkyl chain promoted the formation of bilayer domains, whose width is in agreement with the experimental results.

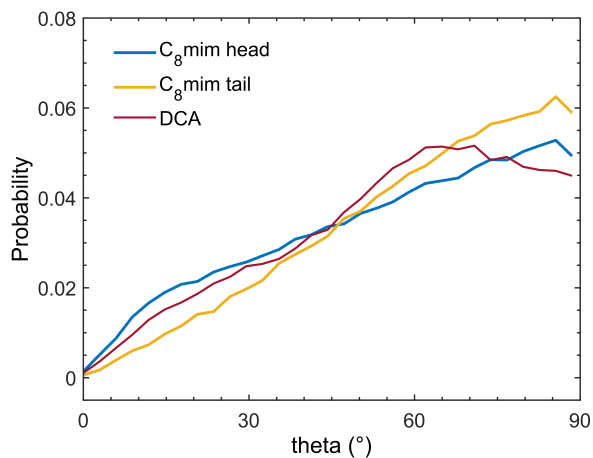


Figure 9: Angular distributions of the $C_8\text{mimDCA}$ system containing 20 000 ppm of water with SiO_2 . The angles plotted are between the plane of the imidazolium ring and the SiO_2 surface, between the end-to-end vector of the octyl side chain and the surface, and between the planes of the DCA and the surface. The distribution includes the imidazolium rings and DCA that were within 1 nm of the surface, and the octyl tails that were within 2 nm of the surface.

Discussion

The agreement between the experimental force curves and the numerical density profiles is remarkable both on MoS₂ and on silica, as shown on Figure 10 and in the Supporting Information (Figures S8 and S9). Both approaches were thus mutually validated and brought complementary pieces of information.

The MD simulation results showed that the thin layers observed on MoS₂ contained a mixture of cations and anions oriented parallel to the substrate, which explained the small size of these layers. The lateral heterogeneity of the ionic layers, evidenced in the simulation snapshots (Figures 5 and 8), explained the variability of the experimental curves for repeated approaches. Indeed, as the radius of curvature of the AFM tip is of the order of 10 times the ion-pair diameter D , our experiment is sensitive to the variations of the local organization of the ions between successive approach and retraction cycles. These variations are due to the thermal diffusion of the surface nanostructures,⁷⁴ to the flow induced by the motion of the AFM cantilever, and to the slow thermal drift of the contact point.

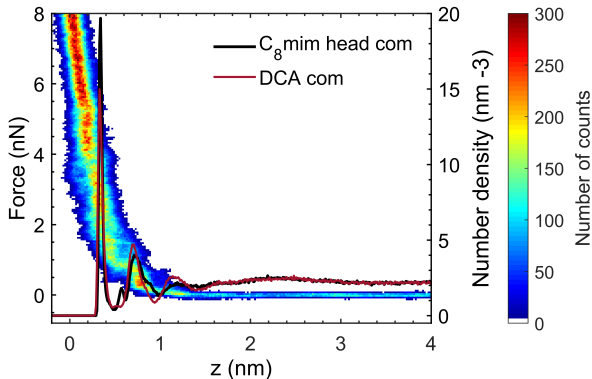


Figure 10: MD density profiles of the dry C₈mimDCA system on MoS₂, superposed to the corresponding AFM 2D force versus separation histogram, measured with a water content of 4000 ppm.

In the experiments on MoS₂, a weak wide layer was detected in the wet system (40 000 ppm water, Figure 3 and S5), but not in the drier system (4000 ppm water, Figure 2 bottom right and S5). The location of this layer

matched reasonably the position of the polar domain found around 2.3 nm in the MoS₂ simulations (see Figure S9). This observation was again in good agreement with the simulations, where the polar domain was indeed reinforced on the right side of the simulation cell in the presence of water, giving an experimental validation of this feature.

Finally, the position of the water peak between the right wall and the first peak of the ionic moieties in the wet silica system, located at 0.2 nm from the substrate, matched the location of layer 1a on the 2D histograms on MoS₂, giving strength to the hypothesis that layer 1a was due to water molecules squeezed between the MoS₂ and the AFM tip. Beware that this position does not correspond to the position of the first water peak in the wet C₈mimDCA/MoS₂ simulation: at equilibrium, the water molecules are located around 0.3 nm from the substrate, that's to say closer to the charged species.

The interfacial structures observed in the experiments and the simulations for the long-chain ILs can be classified into 3 groups, depicted in Figure 11.

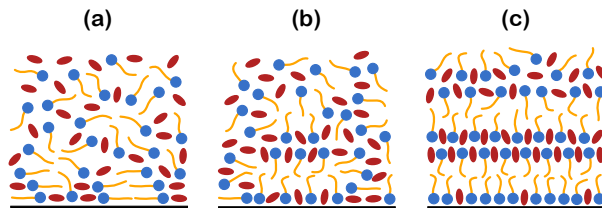


Figure 11: Sketches of 3 kinds of interfacial structures for C₈mimDCA: (a) a thin layer structure, (b) a mixed structure, and (c) a multiple bilayer structure. The imidazolium heads are drawn as blue circles, the alkyl tails as orange lines, and the anions as red ovals.

The first type is a structure composed of thin layers, where each layer is a neutral mixture of anions and cations oriented parallel to the substrate, with very few alkyl chains oriented perpendicularly to the substrate. In this configuration, no thick layer was experimentally detected in the system. In our experiments, this structure was observed on Si treated with HF and dry MoS₂, two apolar and hydrophobic

substrates that are known to have favourable hydrophobic interactions with hydrocarbon contaminants.^{41,75} A similar kind of structure was already reported in a combined AFM and MD study for 1-hexyl-3-methylimidazolium bis(trifluoromethylsulfonyl)imide ($C_6\text{mimNTf}_2$) on amorphous indium gallium zinc oxide (IGZO) by Black *et al.*,¹⁹ and in MD simulations for $C_6\text{mim}$ tetrafluoroborate (BF_4) on graphene by Jo *et al.*⁴⁵ In both cases, it was observed when no potential was applied on the substrates, so that they also belong to the neutral and apolar category.

The second type is a mixed structure with a higher number of alkyl chains oriented perpendicularly to the substrate in the first layer, and belonging to apolar domains. As a result, bilayer patches appear on the substrate, so that the interfacial structure looks more similar to the bulk nanostructure. In the experiments, those bilayer patches, detected as very weak thick layers, may reorganize into thin parallel layers when compressed by the cantilever tip. This structure was observed with $C_8\text{mimDCA}$ on SiO_2 and wet MoS_2 . The same kind of structure was also observed by Mao *et al.*⁶⁰ They performed AFM experiments on a highly oriented pyrolytic graphite (HOPG) electrode with a different type of amphiphilic ionic liquid, with a short chain imidazolium cation and an anion bearing two bulky hydrocarbon groups: 1-butyl-3-methylimidazolium 1,4-bis(2-ethylhexoxy)-1,4-dioxobutane-2-sulfonate ($C_4\text{mimAOT}$). They observed a thin inner layer (with a thickness of about 0.5 nm), and an extremely weak thick layer at open circuit potential. Unfortunately, the water content was not indicated. A similar structure was reported by Cheng *et al.*⁷⁶ for $C_8\text{mim}$ chloride on self-assembled monolayers (SAMs) grafted on a gold substrate. Interestingly, two kinds of SAMs were tested in that study, one hydrophobic terminated by an apolar methyl group, and one hydrophilic terminated by a polar hydroxyl group. The interfacial structure was investigated by AFM for various water contents. At a bulk water content of about 10 000 ppm (which was the drier case), two weak thick layers were detected, which had

the same size but were much weaker than the bilayers observed on a mica substrate at a similar water content in the same study.

The third type is a multiple bilayer structure, with all alkyl chains oriented perpendicular to the substrate in the first layer. The structuration into lamellar apolar and polar domains propagates in several increasingly disordered layers toward the bulk IL. This structure was observed in many experiments with long-chain ionic liquids on mica,^{25,26,32,76} including ours. It was also observed for $C_4\text{mimAOT}$ on HOPG when a potential of ± 1 V was applied on the HOPG electrode by Mao *et al.*,⁶⁰ and for 1-decyl-3-methylimidazolium bis(oxalato)borate ($C_{10}\text{mimBOB}$) on both positively and negatively charged substrates by Watanabe *et al.*³³

Our numerical simulations evidenced the major importance of the chemical nature of the substrate for the IL interfacial structure, since very different structures were obtained for pure ILs on different substrates. For the long chain $C_8\text{mimDCA}$, a thin layer structure was obtained on MoS_2 , while a mixed structure with a large bilayer fraction was obtained on silica. Both simulated substrates were globally neutral in the simulations, but MoS_2 was non polar but polarizable, while the silica substrate was strongly polar, with a fixed polarization. The apolar MoS_2 substrate had not only an attractive hydrophobic interaction with the alkyl chains, but also a strong attractive interaction with the imidazolium ring. Actually, it was strong enough that this positively charged group stayed at the MoS_2 surface even under an applied positive potential, as shown in a previous work.⁴⁶ As a result, this substrate favored a parallel configuration for the long-chain imidazolium cation. Note that a similar argument was also used by Jo *et al.*⁴⁵ to explain the parallel orientation of $C_6\text{mim}$ on graphene, as it has not only an attractive interaction with the alkyl chain, but also a strong $\pi - \pi$ interaction with the imidazolium ring. On the other hand, polar silica attracted polar moieties and repulsed the apolar chains, thus favoring a perpendicular orientation of the cations at the substrate, that promoted the formation of bilayer regions. In both systems, DCA anions were present in the

first layer close to the substrate in the same quantity as imidazolium heads, so that electroneutrality was preserved.

When increasing the bulk water content, the interfacial structure went from a thin layer structure to a mixed one on MoS₂. We attribute this effect to a water-induced strengthening of the segregation of the long-chain IL into polar and apolar nanodomains. But even at 20 000 ppm of water, the bilayer coverage of the interface remained smaller than the one obtained with a silica surface, so that the influence of water impurities was weaker than the one of the substrate's polarity in the simulations.

Finally, the multiple bilayers structure observed on mica may be attributed to a very high negative surface charge. Indeed, mica tends to acquire a high surface charge density due to the dissociation of potassium ions from the 001 cleavage plane in standard handling conditions in a humid atmosphere, with a maximal charge of about 2 electrons per nm².^{77,78} This charge can be compensated by a dense packing of imidazolium heads at the interface, orienting their long alkyl tails away from the interface. The resulting dense forest of alkyl chains would then template the formation of multiple bilayers. Such structures were also observed on other types of charged substrates, either polarized by an applied potential,⁶⁰ or at the surface of salt crystals.³³ Interestingly, bilayers were not observed in a very dry C₈mimNTf₂/mica system in SFA investigations performed by Cheng *et al.*,⁵⁵ that evidenced that water is a necessary ingredient for the formation of bilayers on mica. In their dry system, their force-separation profile was interpreted as resulting from the squeezing of the bulk nanostructure. That observation matches our classification if the potassium ions remain on top of the cleavage plane in absence of water, resulting in a polar and neutral (or weakly charged) surface.

Conclusions

In conclusion, our combined experimental and numerical study allowed to validate our methods and elucidate the EDL structure of a long-

chain IL on different kinds of surfaces, as well as the role of water impurities.

On the one hand, neutral and weakly polar (thus hydrophobic) substrates such as HF-treated Si or MoS₂, that have strong interactions both with the alkyl tail and the imidazolium ring of the cation, promote a parallel orientation of the cation with respect to the substrate, into thin ionic layers that are neutral mixtures of cations and anions. On the other hand, a substrate with a high negative surface charge promotes a perpendicular orientation of the cations at the interface and the segregation of the IL into a succession of lamellar polar and apolar domains. A heterogeneous structure with loose bilayer patches, which may reorganize into thin parallel layers under pressure, is found on an intermediate polar substrate.

A heterogeneous structure is also found on a hydrophobic substrate at high bulk water content, due to the water-enhanced segregation of a long-chain IL into polar and apolar nanodomains. This latter mechanism is rather weak, so that the EDL structure on MoS₂ remains quite robust to water impurities even for a long chain IL, which might have interesting implications for lubrication and iontronic applications.

We expect the behaviour we have evidenced and rationalized on C₈mimDCA to be valid for a wide range of long-chain imidazolium based ILs and substrates, since the interactions of both parts of the cations with the substrate play a central role in the understanding of the IL structure at the interface. This hypothesis seems so far confirmed by the fact that results obtained by other groups with other combinations of long-chain imidazoliums ILs and substrates fit with our proposed classification. The ideas governing this rationalization could be exported to other kinds of long-chain ILs such as C₄mimAOT, and maybe even to some short-chain ionic liquids. For example, they could provide a framework to explain the transition from a long-range organization in alternate cation and anion layers on mica, to a structure with no long-range order on an uncharged SAM-coated mica, as was observed in the SFA experiments of Bou-Malham *et al.*⁵² with two

short chain ILs. It would therefore be interesting to further check this hypothesis by playing with the IL nature and with the surface charge using an applied potential, at various bulk water contents.

Acknowledgement The authors thank S. Cadot and B. Chatmaneerungcharoen for their pioneering work in the preparation of the MoS₂ substrates. They also thank the Agence Nationale de la Recherche for supporting financially this work (Grant No. ANR-18-CE09-0018). A.S. thanks the Liquids and Interfaces team at iLM - UMR5306, for scientific discussions.

Supporting Information Available

Additional XPS and AFM characterization of the substrates, acquisition parameters and bulk water content of the AFM experiments, and structure of the simulated silica substrate. Additional AFM figures, MD results for C₂mimDCA, and direct comparison between MD density profiles and AFM histograms for the SiO₂ and wet MoS₂ systems.

References

- (1) Krossing, I.; Slattery, J. M.; Daguene, C.; Dyson, P. J.; Oleinikova, A.; Weingärtner, H. Why are ionic liquids liquid? A simple explanation based on lattice and solvation energies. *Journal of the American Chemical Society* **2006**, *128*, 13427–13434.
- (2) Endres, F.; El Abedin, S. Z. Air and water stable ionic liquids in physical chemistry. *Physical chemistry chemical physics* **2006**, *8*, 2101–2116.
- (3) Fedorov, M. V.; Kornyshev, A. A. Ionic liquids at electrified interfaces. *Chemical reviews* **2014**, *114*, 2978–3036.
- (4) Maton, C.; De Vos, N.; Stevens, C. V. Ionic liquid thermal stabilities: decomposition mechanisms and analysis tools. *Chemical Society Reviews* **2013**, *42*, 5963–5977.
- (5) MacFarlane, D. R.; Tachikawa, N.; Forsyth, M.; Pringle, J. M.; Howlett, P. C.; Elliott, G. D.; Davis, J. H.; Watanabe, M.; Simon, P.; Angell, C. A. Energy applications of ionic liquids. *Energy & Environmental Science* **2014**, *7*, 232–250.
- (6) Watanabe, M.; Thomas, M. L.; Zhang, S.; Ueno, K.; Yasuda, T.; Dokko, K. Application of ionic liquids to energy storage and conversion materials and devices. *Chemical reviews* **2017**, *117*, 7190–7239.
- (7) Bisri, S. Z.; Shimizu, S.; Nakano, M.; Iwasa, Y. Endeavor of Iontronics: From Fundamentals to Applications of Ion-Controlled Electronics. *Advanced Materials* **2017**, *29*, 1607054.
- (8) Somers, A.; Howlett, P.; MacFarlane, D.; Forsyth, M. A Review of Ionic Liquid Lubricants. *Lubricants* **2013**, *1*, 3–21.
- (9) He, Y.; Li, H.; Qu, C.; Cao, W.; Ma, M. Recent understanding of solid-liquid friction in ionic liquids. *Green Chemical Engineering* **2021**, *2*, 145–157.
- (10) Horn, R.; Evans, D.; Ninham, B. Double-layer and solvation forces measured in a molten salt and its mixtures with water. *The Journal of Physical Chemistry* **1988**, *92*, 3531–3537.
- (11) Oldham, K. B. A Gouy–Chapman–Stern model of the double layer at a (metal)/(ionic liquid) interface. *Journal of Electroanalytical Chemistry* **2008**, *613*, 131–138.
- (12) Hunt, P. A.; Ashworth, C. R.; Matthews, R. P. Hydrogen bonding in ionic liquids. *Chemical Society Reviews* **2015**, *44*, 1257–1288.

- (13) Ray, A. Solvophobic interactions and micelle formation in structure forming non-aqueous solvents. *Nature* **1971**, *231*, 313–315.
- (14) Lauw, Y.; Horne, M.; Rodopoulos, T.; Leermakers, F. Room-temperature ionic liquids: excluded volume and ion polarizability effects in the electrical double-layer structure and capacitance. *Physical review letters* **2009**, *103*, 117801.
- (15) Santos, C. S.; Baldelli, S. Gas–liquid interface of room-temperature ionic liquids. *Chemical Society Reviews* **2010**, *39*, 2136–2145.
- (16) Iwahashi, T.; Sakai, Y.; Kanai, K.; Kim, D.; Ouchi, Y. Alkyl-chain dividing layer at an alcohol/ionic liquid buried interface studied by sum-frequency generation vibrational spectroscopy. *Physical Chemistry Chemical Physics* **2010**, *12*, 12943–12946.
- (17) Hayes, R.; Warr, G. G.; Atkin, R. Structure and nanostructure in ionic liquids. *Chemical reviews* **2015**, *115*, 6357–6426.
- (18) Silvester, D. S.; Jamil, R.; Doblinger, S.; Zhang, Y.; Atkin, R.; Li, H. Electrical Double Layer Structure in Ionic Liquids and Its Importance for Supercapacitor, Battery, Sensing, and Lubrication Applications. *The Journal of Physical Chemistry C* **2021**, *125*, 13707–13720.
- (19) Black, J. M.; Come, J.; Bi, S.; Zhu, M.; Zhao, W.; Wong, A. T.; Noh, J. H.; Pudasaini, P. R.; Zhang, P.; Okatan, M. B., et al. Role of electrical double layer structure in ionic liquid gated devices. *ACS applied materials & interfaces* **2017**, *9*, 40949–40958.
- (20) Misra, R.; McCarthy, M.; Hebard, A. F. Electric field gating with ionic liquids. *Applied Physics Letters* **2007**, *90*, 052905.
- (21) Smith, A. M.; Lovelock, K. R. J.; Gosvami, N. N.; Welton, T.; Perkin, S. Quantized friction across ionic liquid thin films. *Phys. Chem. Chem. Phys.* **2013**, *15*, 15317–15320.
- (22) Lhermerout, R.; Perkin, S. A new methodology for a detailed investigation of quantized friction in ionic liquids. *Phys. Chem. Chem. Phys.* **2020**, *22*, 455–466.
- (23) Sweeney, J.; Hausen, F.; Hayes, R.; Webber, G. B.; Endres, F.; Rutland, M. W.; Bennewitz, R.; Atkin, R. Control of Nanoscale Friction on Gold in an Ionic Liquid by a Potential-Dependent Ionic Lubricant Layer. *Phys. Rev. Lett.* **2012**, *109*, 155502.
- (24) Bresme, F.; Kornyshev, A.; Perkin, S.; Urbakh, M. Electrotunable friction with ionic liquid lubricants. *Nature Materials* **2022**, *21*, 848–858.
- (25) Perkin, S.; Crowhurst, L.; Niedermeyer, H.; Welton, T.; Smith, A. M.; Gosvami, N. N. Self-assembly in the electrical double layer of ionic liquids. *Chemical Communications* **2011**, *47*, 6572–6574.
- (26) Smith, A. M.; Lovelock, K. R.; Gosvami, N. N.; Licence, P.; Dolan, A.; Welton, T.; Perkin, S. Monolayer to bilayer structural transition in confined pyrrolidinium-based ionic liquids. *The journal of physical chemistry letters* **2013**, *4*, 378–382.
- (27) Garcia, L.; Jacquot, L.; Charlaix, E.; Cross, B. Nano-mechanics of ionic liquids at dielectric and metallic interfaces. *Faraday Discuss.* **2018**, *206*, 443–457.
- (28) Han, M.; Kim, H.; Leal, C.; Negrito, M.; Batteas, J. D.; Espinosa-Marzal, R. M. Insight into the Electrical Double Layer of Ionic Liquids Revealed through Its Temporal Evolution. *Advanced Materials Interfaces* **2020**, *7*, 2001313.
- (29) Atkin, R.; El Abedin, S. Z.; Hayes, R.; Gasparotto, L. H.; Borisenko, N.; Endres, F. AFM and STM studies on the surface interaction of [BMP] TFSA and [EMIm] TFSA ionic liquids with Au (111).

- (30) Hayes, R.; Borisenko, N.; Tam, M. K.; Howlett, P. C.; Endres, F.; Atkin, R. Double layer structure of ionic liquids at the Au (111) electrode interface: an atomic force microscopy investigation. *The Journal of Physical Chemistry C* **2011**, *115*, 6855–6863.
- (31) Black, J. M.; Walters, D.; Labuda, A.; Feng, G.; Hillesheim, P. C.; Dai, S.; Cummings, P. T.; Kalinin, S. V.; Proksch, R.; Balke, N. Bias-dependent molecular-level structure of electrical double layer in ionic liquid on graphite. *Nano Letters* **2013**, *13*, 5954–5960.
- (32) Griffin, L. R.; Browning, K. L.; Clarke, S. M.; Smith, A. M.; Perkin, S.; Skoda, M. W. A.; Norman, S. E. Direct measurements of ionic liquid layering at a single mica–liquid interface and in nano-films between two mica–liquid interfaces. *Phys. Chem. Chem. Phys.* **2017**, *19*, 297–304.
- (33) Watanabe, S.; Pilkington, G. A.; Oleshkevych, A.; Pedraz, P.; Radiom, M.; Welbourn, R.; Glavatskih, S.; Rutland, M. W. Interfacial structuring of non-halogenated imidazolium ionic liquids at charged surfaces: effect of alkyl chain length. *Phys. Chem. Chem. Phys.* **2020**, *22*, 8450–8460.
- (34) Klein, J. M.; Squire, H.; Gurkan, B. Electroanalytical Investigation of the Electrode–Electrolyte Interface of Quaternary Ammonium Ionic Liquids: Impact of Alkyl Chain Length and Ether Functionality. *The Journal of Physical Chemistry C* **2019**, *124*, 5613–5623.
- (35) Zhang, M.; Duan, S.; Luo, S.; Zhong, Y.; Yan, J.; Liu, G.; Mao, B.; Tian, Z. Structural Exploration of Multilayered Ionic Liquid/Ag Electrode Interfaces by Atomic Force Microscopy and Surface-Enhanced Raman Spectroscopy. *ChemElectroChem* **2020**, *7*, 4936–4942.
- (36) Sitaputra, W.; Stacchiola, D.; Wishart, J. F.; Wang, F.; Sadowski, J. T. In situ probing of ion ordering at an electrified ionic liquid/Au interface. *Advanced Materials* **2017**, *29*, 1606357.
- (37) Romero, C.; Moore, H. J.; Lee, T. R.; Baldelli, S. Orientation of 1-butyl-3-methylimidazolium based ionic liquids at a hydrophobic quartz interface using sum frequency generation spectroscopy. *The Journal of Physical Chemistry C* **2007**, *111*, 240–247.
- (38) Romero, C.; Baldelli, S. Sum frequency generation study of the room-temperature ionic liquids/quartz interface. *The Journal of Physical Chemistry B* **2006**, *110*, 6213–6223.
- (39) Rodenbücher, C.; Wippermann, K.; Korte, C. Atomic force spectroscopy on ionic liquids. *Applied Sciences* **2019**, *9*, 2207.
- (40) Fukui, K.-i. Development of local analysis technique of electric double layer at electrode interfaces and its application to ionic liquid interfaces. *Bulletin of the Chemical Society of Japan* **2018**, *91*, 1210–1219.
- (41) Uhlig, M. R.; Martin-Jimenez, D.; Garcia, R. Atomic-scale mapping of hydrophobic layers on graphene and few-layer MoS₂ and WSe₂ in water. *Nature communications* **2019**, *10*, 1–7.
- (42) Zhou, S.; Panse, K. S.; Motevaselian, M. H.; Aluru, N. R.; Zhang, Y. Three-Dimensional Molecular Mapping of Ionic Liquids at Electrified Interfaces. *ACS nano* **2020**, *14*, 17515–17523.
- (43) Umeda, K.; Kobayashi, K.; Minato, T.; Yamada, H. Atomic-Scale Three-Dimensional Local Solvation Structures of Ionic Liquids. *The Journal of Physical Chemistry Letters* **2020**, *11*, 1343–1348.

- (44) Liu, X.; Wang, Y.; Li, S.; Yan, T. Effects of anion on the electric double layer of imidazolium-based ionic liquids on graphite electrode by molecular dynamics simulation. *Electrochimica Acta* **2015**, *184*, 164–170.
- (45) Jo, S.; Park, S. W.; Shim, Y.; Jung, Y. J. Effects of Alkyl Chain Length on Interfacial Structure and Differential Capacitance in Graphene Supercapacitors: A Molecular Dynamics Simulation Study. *Electrochimica Acta* **2017**, *247*, 634–645.
- (46) Gong, Z.; Padua, A. A. H. Effect of side chain modifications in imidazolium ionic liquids on the properties of the electrical double layer at a molybdenum disulfide electrode. *The Journal of Chemical Physics* **2021**, *154*, 084504.
- (47) Merlet, C.; Rotenberg, B.; Madden, P. A.; Salanne, M. Computer simulations of ionic liquids at electrochemical interfaces. *Phys. Chem. Chem. Phys.* **2013**, *15*, 15781–15792.
- (48) Voeltzel, N.; Fillot, N.; Vergne, P.; Joly, L. Orders of Magnitude Changes in the Friction of an Ionic Liquid on Carbonaceous Surfaces. *The Journal of Physical Chemistry C* **2018**, *122*, 2145–2154.
- (49) Di Lecce, S.; Kornyshev, A. A.; Urbakh, M.; Bresme, F. Structural effects in nanotribology of nanoscale films of ionic liquids confined between metallic surfaces. *Phys. Chem. Chem. Phys.* **2021**, *23*, 22174–22183.
- (50) Page, A. J.; Elbourne, A.; Stefanovic, R.; Addicoat, M. A.; Warr, G. G.; Voitchovsky, K.; Atkin, R. 3-Dimensional atomic scale structure of the ionic liquid–graphite interface elucidated by AM-AFM and quantum chemical simulations. *Nanoscale* **2014**, *6*, 8100–8106.
- (51) Black, J. M.; Zhu, M.; Zhang, P.; Unocic, R. R.; Guo, D.; Okatan, M. B.; Dai, S.; Cummings, P. T.; Kalinin, S. V.; Feng, G.; Balke, N. Fundamental aspects of electric double layer force-distance measurements at liquid-solid interfaces using atomic force microscopy. *Scientific Reports* **2016**, *6*, 32389.
- (52) Bou-Malham, I.; Bureau, L. Nanoconfined ionic liquids: effect of surface charges on flow and molecular layering. *Soft Matter* **2010**, *6*, 4062–4065.
- (53) Atkin, R.; Borisenko, N.; Druschler, M.; Endres, F.; Hayes, R.; Huber, B.; Rolling, B. Structure and dynamics of the interfacial layer between ionic liquids and electrode materials. *Journal of Molecular Liquids* **2014**, *192*, 44–54.
- (54) Sheehan, A.; Jurado, L. A.; Ramakrishna, S. N.; Arcifa, A.; Rossi, A.; Spencer, N. D.; Espinosa-Marzal, R. M. Layering of ionic liquids on rough surfaces. *Nanoscale* **2016**, *8*, 4094–4106.
- (55) Cheng, H.-W.; Dienemann, J.-N.; Stock, P.; Merola, C.; Chen, Y.-J.; Valtiner, M. The effect of water and confinement on self-assembly of imidazolium based ionic liquids at mica interfaces. *Scientific reports* **2016**, *6*, 1–9.
- (56) Jurado, L. A.; Kim, H.; Rossi, A.; Arcifa, A.; Schuh, J. K.; Spencer, N. D.; Leal, C.; Ewoldt, R. H.; Espinosa-Marzal, R. M. Effect of the environmental humidity on the bulk, interfacial and nanoconfined properties of an ionic liquid. *Phys. Chem. Chem. Phys.* **2016**, *18*, 22719–22730.
- (57) Zhong, Y.; Yan, J.; Li, M.; Chen, L.; Mao, B. The electric double layer in an ionic liquid incorporated with water molecules: atomic force microscopy force curve study. *ChemElectroChem* **2016**, *3*, 2221–2226.
- (58) Qiao, R. Water at ionic liquids-solid interfaces. *Current Opinion in Electrochemistry* **2019**, *13*, 11–17.

- (59) Niemann, T.; Li, H.; Warr, G.; Ludwig, R.; Atkin, R. Influence of Hydrogen Bonding Between Ions of Like Charge on the Ionic Liquid Interfacial Structure at a Mica Surface. *The Journal of Physical Chemistry Letters* **2019**, XXXX.
- (60) Mao, X.; Brown, P.; Červinka, C.; Hazell, G.; Li, H.; Ren, Y.; Chen, D.; Atkin, R.; Eastoe, J.; Grillo, I.; Padua, A. A.; Costa Gomes, M.; Hutton, T. A. Self-assembled nanostructures in ionic liquids facilitate charge storage at electrified interfaces. *Nature Materials* **2019**, *18*, 1350–1357.
- (61) Perera, M. M.; Lin, M.-W.; Chuang, H.-J.; Chamlagain, B. P.; Wang, C.; Tan, X.; Cheng, M. M.-C.; Tománek, D.; Zhou, Z. Improved Carrier Mobility in Few-Layer MoS₂ Field-Effect Transistors with Ionic-Liquid Gating. *ACS Nano* **2013**, *7*, 4449–4458, PMID: 23590723.
- (62) Mantina, M.; Chamberlin, A. C.; Valero, R.; Cramer, C. J.; Truhlar, D. G. Consistent van der Waals Radii for the Whole Main Group. *J. Phys. Chem. A* **2009**, *113*, 5806–5812.
- (63) Cadot, S.; Renault, O.; Frégnaux, M.; Rouchon, D.; Nolot, E.; Szeto, K.; Thieuleux, C.; Veyre, L.; Okuno, H.; Martin, F., et al. A novel 2-step ALD route to ultra-thin MoS₂ films on SiO₂ through a surface organometallic intermediate. *Nanoscale* **2017**, *9*, 538–546.
- (64) Higgins, M. J.; Proksch, R.; Sader, J. E.; Polcik, M.; Mc Endoo, S.; Cleveland, J. P.; Jarvis, S. P. Noninvasive determination of optical lever sensitivity in atomic force microscopy. *Review of Scientific Instruments* **2006**, *77*, 013701.
- (65) Goloviznina, K.; Canongia Lopes, J. N.; Costa Gomes, M.; Pádua, A. A. Transferable, Polarizable Force Field for Ionic Liquids. *Journal of Chemical Theory and Computation* **2019**, *15*, 5858–5871.
- (66) Lamoureux, G.; Harder, E.; Vorobyov, I. V.; Roux, B.; MacKerell, A. D. A polarizable model of water for molecular dynamics simulations of biomolecules. *Chemical Physics Letters* **2006**, *418*, 245–249.
- (67) Cygan, R. T.; Liang, J.-J.; Kalinichev, A. G. Molecular Models of Hydroxide, Oxyhydroxide, and Clay Phases and the Development of a General Force Field. *The Journal of Physical Chemistry B* **2004**, *108*, 1255–1266.
- (68) Sresht, V.; Govind Rajan, A.; Bordes, E.; Strano, M. S.; Padua, A. A. H.; Blankschtein, D. Quantitative Modeling of MoS₂-Solvent Interfaces: Predicting Contact Angles and Exfoliation Performance using Molecular Dynamics. *The Journal of Physical Chemistry C* **2017**, *121*, 9022–9031.
- (69) Yeh, I. C.; Berkowitz, M. L. Ewald summation for systems with slab geometry. *The Journal of Chemical Physics* **1999**, *111*, 3155–3155.
- (70) Eastman, Peter, Friedrichs, Mark S., Chodera, John D., Radmer, Randall J., Brunts, Christopher M., Ku, Joy P., Beauchamp, Kyle A., Lane, Thomas J., Wang, Lee-Ping, Shukla, Diwakar, Tye, Tony, Houston, Mike, Stich, Timo, Klein, Christoph, Shirts, Mciachel R, V. S. OpenMM 4: A Reusable, Extensible, Hardware Independent Library for High Performance Molecular Simulation. *Journal of Chemical Theory and Computation* **2013**, *9*, 461–469.
- (71) Eastman, P.; Swails, J.; Chodera, J. D.; McGibbon, R. T.; Zhao, Y.; Beauchamp, K. A.; Wang, L. P.; Simonett, A. C.; Harrigan, M. P.; Stern, C. D.; Wiewiora, R. P.; Brooks, B. R.; Pande, V. S. OpenMM 7: Rapid development of high performance algorithms for molecular dynamics. *PLoS Computational Biology* **2017**, *13*, 1–17.

- (72) Payal, R. S.; Balasubramanian, S. Effect of cation symmetry on the organization of ionic liquids near a charged mica surface. *Journal of Physics: Condensed Matter* **2014**, *26*, 284101.
- (73) Hoth, J.; Hausen, F.; Müser, M. H.; Bennewitz, R. Force microscopy of layering and friction in an ionic liquid. *Journal of Physics: Condensed Matter* **2014**, *26*, 284110.
- (74) Li, H.; Wang, J.; Warr, G. G.; Atkin, R. Extremely slow dynamics of ionic liquid self-assembled nanostructures near a solid surface. *Journal of Colloid and Interface Science* **2023**, *630*, 658–665.
- (75) Grundner, M.; Jacob, H. Investigations on hydrophilic and hydrophobic silicon (100) wafer surfaces by X-ray photoelectron and high-resolution electron energy loss-spectroscopy. *Applied Physics A* **1986**, *39*, 73–82.
- (76) Cheng, H.-W.; Weiss, H.; Stock, P.; Chen, Y.-J.; Reinecke, C. R.; Diemann, J.-N.; Mezger, M.; Valtiner, M. Effect of Concentration on the Interfacial and Bulk Structure of Ionic Liquids in Aqueous Solution. *Langmuir* **2018**, *34*, 2637–2646, PMID: 29356544.
- (77) Christenson, H. K.; Thomson, N. H. The nature of the air-cleaved mica surface. *Surface Science Reports* **2016**, *71*, 367–390.
- (78) Gong, X.; Wang, B.; Kozbial, A.; Li, L. From Molecular Arrangement to Macroscopic Wetting of Ionic Liquids on the Mica Surface: Effect of Humidity. *Langmuir* **2018**, *34*, 12167–12173, PMID: 30230344.

TOC Graphic

